Mechanics of Materials 13 (1992) 67–77
Elsevier

Three-dimensional effects in thin film fracture mechanics

Toshio Nakamura

Department of Mechanical Engineering, State University of New York at Stony Brook, Stony Brook, NY 11794, USA

and

Sundar M. Kamath

IBM General Technology Division, Hopewell Junction, NY 12533, USA

Received 8 July 1991; revised version received 7 November 1991

This paper presents the results of a three-dimensional finite element analysis of the mechanics of crack growth and decohesion in a highly compliant thin film bonded to a rigid substrate. Essential features of the model are a surface-breaking initial crack which has penetrated to the film–substrate interface, and a remote biaxial residual stress field in the film. Computational analyses show that, in the absence of decohesion, the stress intensity factor along the leading edge of the crack reaches a steady state value when the crack is about twice the film thickness. This steady state condition gives rise to a nearly parabolic crack front along the leading edge. The computed results also confirm the existence of high interface stresses that are the driving force for film decohesion. When decohesion is permitted, the stress intensity factor is observed to increase with debond opening angle. The equilibrium state between crack propagation and decohesion may be determined from the respective stress intensity factors and fracture toughness of the film and the interface.

1. Introduction

Thin films or coatings on substrates or fibers are of significant technological importance in applications ranging from micro-electronics to advanced composites for aerospace. Several papers have discussed the mechanics of failures in thin films, as reviewed extensively by Hutchinson and Suo (1991). The primary failure mode can be categorized either as one involving film cracking, or interfacial delamination, or some combination of the two. A "global" analysis of the thin film decohesion problem can be carried out using the nondimensional parameter Ω_c to characterize modes of failure (Evans, Drory and Hu, 1988) as a function of film or interface toughness and film stress. Some success has been reported in applying such ideas for certain classes of film–substrate combinations. However, the approach is semi-empirical in nature and applies to steady state condition only. An analytical description of the conditions leading to the onset of film cracking or delamination is still not available.

While some experimental and analytical studies have addressed the likelihood of decohesion at a macro-scale, no study has yet addressed the three-dimensional aspect of thin film decohesion. However, as seen later in this paper, due to the nature of the resulting deformation field, 3-D effects can be critical to understanding failure modes of thin films. We consider, one, important aspect of 3-D effects in this paper, namely, a 3-D analysis of a thin film crack and related debonding under the influence of biaxial tensile residual stress in the film caused by thermal coefficient mismatch.

A 3-D finite element analysis of the surface flaw problem for a thin film bonded to a rigid

0167-6636/92/$05.00 © 1992 – Elsevier Science Publishers B.V. All rights reserved

substrate was reported by Hu et al. (1991). Recently, Beuth (1991) presented various results for a thin film crack oriented perpendicular to the film–substrate interface. His solutions based on a plane strain analysis can be used to predict several modes of cracking in a thin film subjected to residual tension. In this study, detailed 3-D finite element computations are performed to investigate the complete stress field surrounding a similarly oriented crack. Our primary goal is to determine the effects of crack length and debond opening angle on the crack driving force in the thin film subjected to residual stress. We will also clarify essential 3-D features associated with the mechanics of thin film fracture.

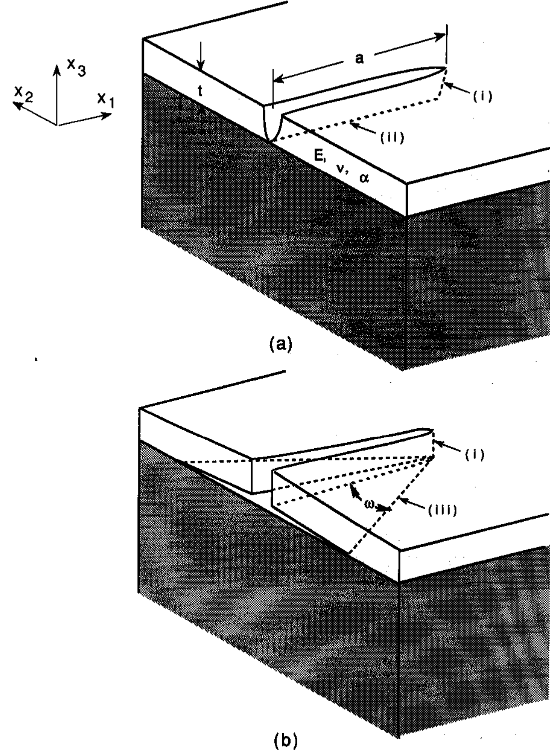

Fig. 1. Schematic of half-model of thin film on a substrate containing: (a) a bonded crack, (b) a debonded crack with debond opening angle, ω. Definition of three types of crack fronts are indicated in the figure.

2. Crack tip field for thermal stress state

2.1. Singular stress fields

The stress–strain relation of an isotropic linear elastic material, under thermal stresses is

$$\sigma_{ij} = \frac{E}{1+\nu}\epsilon_{ij} + \frac{\nu E}{(1+\nu)(1-2\nu)}\delta_{ij}\epsilon_{kk} - \frac{E\alpha}{1-2\nu}\delta_{ij}T. \quad (1)$$

Here E is the Young's modulus, ν is the Poisson's ratio, α is linear coefficient of thermal expansion, and T is the temperature deviation from the reference value at undeformed state.

In the thin film–substrate model considered here, there are three possible crack front configurations as illustrated in Fig. 1. They are: (i) a homogeneous crack front within the thin film, whose propagation enlarges the crack surface length, (ii) a crack front directed downward to the substrate and impinges the interface plane, and (iii) an interface crack front of a delaminated plane between the film and substrate. In the model without decohesion, types (i) and (ii) exist as shown in Fig. 1a while types (i) and (iii) are present in the model with decohesion as shown in Fig. 1b. The asymptotic stress field of each type is briefly described below.

For a homogeneous crack propagating through the thin film (type (i)), the stress field very close to the crack front is given by the usual K-field solution as

$$\sigma_{ij}(r, \theta) = \frac{K_{\mathrm{I}}}{\sqrt{2\pi r}} f_{ij}(\theta), \quad (2)$$

where r and θ are the in-plane coordinates of the plane normal to the crack front, K_{I} is the Mode I stress intensity factor and f_{ij} are the angular variations of stress components for plane strain condition. The above equation is valid under thermal loading condition so long as the temperature field remains bounded.

When the crack is directed normal to the substrate and terminates at the interface (type

(ii)), the near tip stress field is given by (Cook and Erdogan, 1972; He and Hutchinson, 1989)

$$\sigma_{ij}(r,\theta) = \frac{K_\mathrm{I}}{\sqrt{2\pi}} r^{-\lambda} \hat{\sigma}_{ij}(\theta). \tag{3}$$

Here, K_I has the dimension of [(stress) · (length)$^\lambda$] and $\hat{\sigma}_{ij}$ is the angular variation of stress. The stress singularity coefficient λ is root of the equation containing the material constants of film and substrate (Zak and Williams, 1963)

$$\cos \lambda\pi = \frac{2(\beta-\alpha)}{1+\beta}(1-\lambda)^2 + \frac{\alpha+\beta^2}{1-\beta}. \tag{4}$$

Here, α and β are the Dundurs' parameters (Dundurs, 1969) defined under plane strain condition as,

$$\alpha = \frac{\mu_1(1-\nu_2) - \mu_2(1-\nu_1)}{\mu_1(1-\nu_2) + \mu_2(1-\nu_1)},$$
$$\beta = \frac{\mu_1(1-2\nu_2) - \mu_2(1-2\nu_1)}{2\mu_1(1-\nu_2) + 2\mu_2(1-\nu_1)}, \tag{5}$$

where μ is shear modulus, ν is Poisson's ratio and subscripts 1 and 2 refer to the film and substrate, respectively. In general, if the modulus of material 1 is less than that of material 2, then the stress ahead of crack has lower order singularity than the usual $1/\sqrt{r}$ singularity (i.e., $\lambda < 0.5$).

The asymptotic stress field along the edge of the delamination, type (iii) in Fig. 1b, corresponds to the two-dimensional bimaterial K-field solution. The form of the solution given by Rice, Suo and Wang (1990) is

$$\sigma_{ij} = \frac{1}{\sqrt{2\pi r}}\{\mathrm{Re}[\boldsymbol{K}r^{\mathrm{i}\epsilon}]\tilde{\sigma}_{ij}^{\mathrm{I}}(\theta;\epsilon) + \mathrm{Im}[\boldsymbol{K}r^{\mathrm{i}\epsilon}]\tilde{\sigma}_{ij}^{\mathrm{II}}(\theta;\epsilon) + K_{\mathrm{III}}\tilde{\sigma}_{ij}^{\mathrm{III}}(\theta)\}, \tag{6}$$

where $\boldsymbol{K} = K_\mathrm{I} + \mathrm{i}K_\mathrm{II}$ is defined as the complex stress intensity factor for the in-plane modes, and $\tilde{\sigma}_{ij}$ are the angular variations of stress components for each mode. The oscillatory index ϵ is a material dependent parameter defined as

$$\epsilon = \frac{1}{2\pi}\ln\left(\frac{1-\beta}{1+\beta}\right). \tag{7}$$

Hence, along a three-dimensional crack front, the crack tip field generally contains all three modes for any types of remote loading.

When the material properties of the film and the substrate are the same, i.e., homogeneous case, the stress fields given by (2), (3) and (6) coincide for pure Mode I. In the present film–substrate model, with the Poisson's ratio of the film chosen as $\nu_1 = 0.3$ and the substrate assumed to be rigid, the Dundurs' parameters are $\alpha = -1.0$, $\beta = -0.2857$, the singularity coefficient determined from (4) is $\lambda = 0.2888$ and the oscillatory index from (7) is $\epsilon = 0.0935$.

2.2. Three-dimensional J-integral

In a numerical analysis, the stress intensity factor is most accurately calculated from the J-integral. Along a three-dimensional crack front, J is expressed in terms of near-tip fields as

$$J(s) = \lim_{\Gamma\to 0} \mu_k(s) \int_{\Gamma(s)} \left(W n_k - \sigma_{ij} n_j \frac{\partial u_i}{\partial x_k} \right) \mathrm{d}\Gamma, \tag{8}$$

where s is the location of the crack tip and $\mu_k(s)$ is a unit vector giving the direction which is formed by the intersection of the plane normal to the crack front and the plane tangential to the crack plane at s. The strain energy density W is defined as the mechanical work of strain,

$$W = \tfrac{1}{2}(\sigma_{ij}\epsilon_{ij} - \alpha T \sigma_{kk}). \tag{9}$$

For a linear elastic material, the J-integral is equivalent to the energy release rate.

From a discrete computational point of view, the integral (8) is not suitable for evaluating J, and a more appropriate expression based on a domain integral formulation for thermal stresses was given by Shih, Moran and Nakamura (1986). In their formulation, the total energy release $\bar{J}$ due to a virtual crack extension over a crack front segment δs is computed as

$$\bar{J} = \int_V \left(\sigma_{ij} \frac{\partial u_i}{\partial x_k}\frac{\partial q_k}{\partial x_j} - W\frac{\partial q_k}{\partial x_k} + \alpha\sigma_{ii}\frac{\partial T}{\partial x_k} q_k \right) \mathrm{d}V. \tag{10}$$

Here V is an arbitrary volume which encloses the crack segment, the weighting q_k is a continuous function of position and it equals the direction and magnitude of the virtual crack extension along δs. In the finite element model, each crack front segment is associated with a particular crack front node, and $\bar{J}$ is computed for several domains/volumes. The consistency of $\bar{J}$ from different domains is used as the accuracy check for J. Once $\bar{J}$ is computed, and approximation of $J(s)$ at each nodal point can be obtained from

$$J(s) = \frac{\bar{J}(s)}{\int_{\delta s} q_k(s)\mu_k(s)\,\mathrm{d}s}. \tag{11}$$

A more consistent determination of $J(s)$ from $\bar{J}(s)$ was demonstrated by Shih et al. (1986). In the present analysis, a high stress gradient (along the crack front direction) makes an accurate computation of $\bar{J}$ difficult near the interface crack front node. Therefore, we have used relation (11) to determine $J(s)$ so that any error arising from the interface region does not influence values outside the region. More detailed discussions on the computation of J along a curved crack front are given by Li et al. (1985) and Shih et al. (1986).

The relationship between the stress intensity factor and a local J at a point on a crack front in a homogeneous material, type (i) crack front in Fig. 1a, is given by

$$J = \frac{1-\nu^2}{E}K_{\mathrm{I}}^2. \tag{12}$$

For the type (ii) crack front, J-integral cannot be defined since the singularity is different from $1/\sqrt{r}$. A detailed discussion of the elastic interface crack field, type (iii) crack front in Fig. 1b, including the relationship between the J and the stress intensity factors, can be found in the article by Rice et al. (1990).

3. Analysis of bonded crack

3.1. Model

The first part of this study deals with three-dimensional effects in the absence of decohesion. The film is subjected to residual biaxial tensile stresses induced by the mismatch of thermal expansion coefficients between the film and the substrate during cooling. Initially, the film contains a surface-breaking crack of length $2a$ in a plane perpendicular to the film–substrate interface. The half geometry of film–substrate model is shown in Fig. 1a. It is assumed that the crack has already penetrated to the interface or close to the interface that any effect due to the remaining distance is minimum. Based on a dimensional analysis, the distance between the tip and the interface is given by a function of normalized residual stress, fracture toughness of the film and the material constants (see Hutchinson and Suo, 1991). According to the results given by Beuth (1991), this distance is at most a few percent of the film thickness for the compliant thin film bonded to a rigid substrate. In the bonded crack model, further propagation occurs only along the crack front bounded by the free-surface and the interface.

The Young's modulus of the film is E and the coefficient α represents the *difference* in thermal expansion coefficients between the film and the substrate. Since the elastic modulus of ceramic substrate is much higher than that of the film, we have taken the substrate to be rigid. The Poisson's ratio of the film is chosen to be $\nu = 0.3$. Any nonlinearity in geometry change and material response are not included in this study.

The width and height of the film are taken to be large enough so that the near tip field is independent of the in-plane (x_1–x_2) dimensions. In constructing the finite element mesh, we have used the symmetry condition across the crack and ligament plane and the center plane of the model, so that only a quarter of the thin film geometry is modelled. The origin of Cartesian coordinates is chosen at the bottom of the crack front where it meets the substrate. The film has a thickness t, and it is bounded between $x_3 = 0$ (interface) and $x_3 = t$ (free-surface). Various meshes are constructed for different crack lengths, but always keeping the in-plane dimensions of the film to be larger than $10t$. An accurate calculation of $J(s)$ requires sufficiently small elements along the crack front. In all our models, the element size is

gradually decreased as the radial distance to crack tip decreases, while the angular increment of each mesh is kept constant at $\Delta\theta = \pi/12$ near the crack front. The identical planar mesh is repeated along the x_3-axis. Special care has been taken for choosing optimum thickness of each element layer. In the thin film–substrate problem, the high stress gradient along the crack front is expected not only near the free-surface but also near the interface. To accomodate them, thinner element layers are employed near the free-surface as well as near the interface. The total number of element layers through the thickness ranges from 14 to 17 in the vicinity of the crack front, and it is reduced at remote locations where variations of field quantities through the thickness are small. A typical mesh is shown in Fig. 2. We have used 5000 to 7000 linear 8-noded 3-D elements to construct various quarter-model meshes. The finite element analysis is performed with the ABAQUS code available from Hibbitt, Karlson and Sorenson, Inc., Providence, RI.

Since no decohesion of the film is allowed here, the nodes along the bottom of crack face are tied to the rigid substrate. Residual stress in the film develops when the temperature of all nodal points is lowered. Away from the crack, the state of stress is biaxial tension, $\sigma_{11} = \sigma_{22} = \sigma_0 = -E\alpha T/(1-\nu)$. The direct application of thermal loading offers several advantages over other equivalent methods of computing K_I, such as applying crack face traction or by imposing interface nodal displacements.

3.2. Effect of crack length

Initially, the leading crack front is assumed to be straight and normal to the interface so that it coincides with the x_3-axis. Several computations are performed for different crack lengths in the range $0.2 \leqslant a/t \leqslant 10$. In each case, the stress intensity factor along the crack front is obtained via the J-integral discussed in Section 2.2. Note that "crack front" here refers to the leading edge of crack type (i) in Fig. 1a.

Before discussing the numerical results, we note that the asymptotic structure of stress field near the two end locations ($x_3/t \doteq 0$ and 1) are different from the usual K-field given in (2). At the intersection of the crack front and free-surface ($x_3/t = 1$), Benthem (1977), Bazant and Estenssoro (1979) and others have shown that the asymptotic field has a lower order singularity than $1/\sqrt{r}$ when the angle of the intersection is 90° under Mode I loading condition ($\sim r^{-0.452}$ for $\nu = 0.3$). This implies that K_I must vanish at this

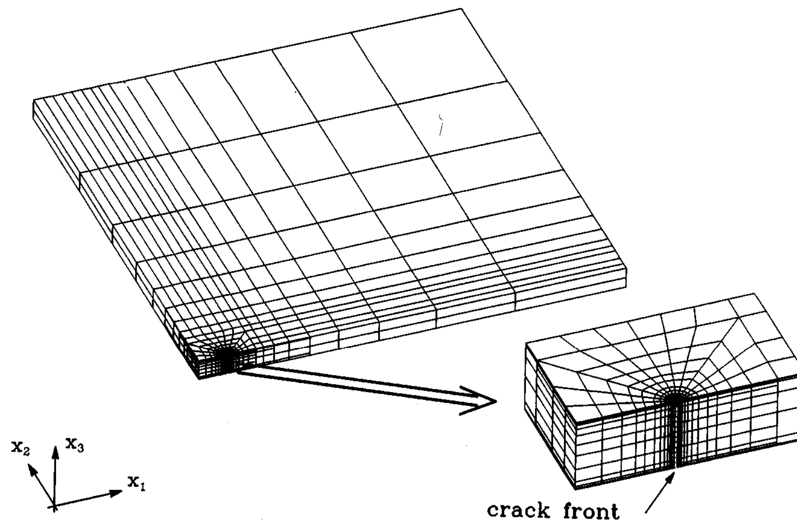

Fig. 2. Finite element mesh for quarter section of thin film model. Near crack front region is magnified.

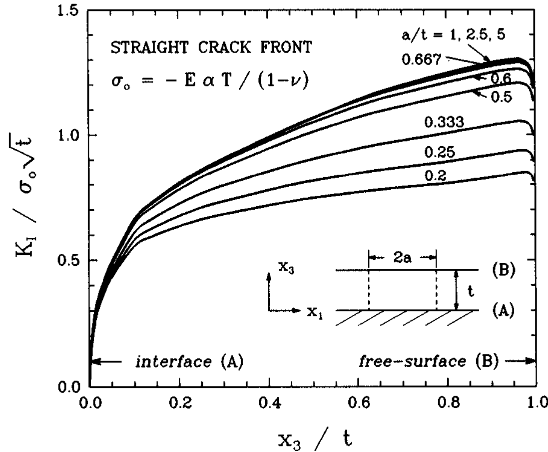

Fig. 3. Stress intensity factor across the thickness of the film for various crack lengths. Cross-section of thin film on crack plane is depicted.

corner point. The order of singularity depends on the Poisson's ratio as well as the angle at which the crack front intersects the free-surface. The size of the corner field was found to be a small fraction ($\approx 1\%$) of thickness in a thin plate with a through-crack (Nakamura and Parks, 1988). At the other end of the crack front ($x_3/t = 0$), the asymptotic behavior of the corner field adjacent to the rigid plane is still unknown. However, it is likely that the corner singularity is weaker than $1/\sqrt{r}$ since the asymptotic field of the crack terminating at the rigid substrate has the singularity $r^{-0.2888}$ (see Section 2.1). Thus, K_I is also expected to vanish at this location. Therefore, for the present crack geometry (i.e., crack front normal to the interface), variation of K_I along the crack front is subjected to the condition $K_\mathrm{I} = 0$ at both ends of the front.

Computed local K_I is normalized by $\sigma_0\sqrt{t}$ and plotted for various crack lengths in Fig. 3. Here σ_0 is the remote biaxial tensile stress due to cooling and expansion mismatch. For all crack lengths, K_I increases with x_3/t until the maximum value of K_I is reached just below the free-surface. The effect of the corner field at free-surface is seen by the drop in K_I very near $x_3/t = 1$. Elsewhere, K_I increases with crack length, until $a \approx t$ when it reaches a plateau and remains unchanged for longer cracks. It is interesting to observe that there is no difference in crack driving force between long and short cracks in compliant thin films once the crack length is approximately twice the film thickness. This can be treated as an "equilibrium" or steady state crack length.

3.3. Curved crack front

As shown in Fig. 3, the steady state crack length is of the same order as the film thickness. No further increase in K_I occurs for longer cracks. If it is assumed that a crack propagates with nearly constant critical energy release rate or stress intensity factor K_Ic along the crack front, then a steady state crack front shape should emerge. It is therefore of interest to know what shape the crack front attains at steady state. The crack front shape/profile corresponding to nearly constant K_I across the thickness is determined using an iterative remeshing of the finite element model. During the remeshing, the crack front nodes are shifted in the x_1 direction based on the difference between K_I at a node and the average K_I for the entire crack front ($K_\mathrm{I}^\mathrm{ave}$). For example, if K_I at a node is higher than $K_\mathrm{I}^\mathrm{ave}$, then its x_1 coordinate is increased proportional to the normalized difference $(K_\mathrm{I} - K_\mathrm{I}^\mathrm{ave})/K_\mathrm{I}^\mathrm{ave}$. The process is carried out for all crack front nodes and repeated for several iterations. During the shifting of the nodes, restrictions are imposed to avoid deterioration of J calculations. The accuracy of J worsens when the angle between a crack front segment and the x_3-axis becomes too large. The maximum tilt angle is set at 60°, and the crack front segments near the interface have reached this limit. It has been observed that the value of K_I at a node depends on its relative x_1 position with respect to the neighboring nodes and not directly on the absolute coordinate. In fact, the variation of K_I is very sensitive to the curvature of the crack front. To determine the shape of the steady state curved crack front, the straight crack front mesh geometry with $a/t = 10$ is chosen as the initial model.

The computed steady state crack front shape is shown in Fig. 4. It is nearly parabolic except near

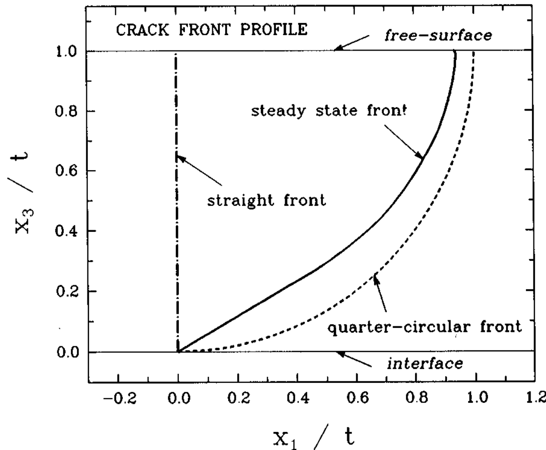

Fig. 4. Crack front profile under steady state propagation in crack center plane $x_2/t = 0$. The quarter-circular shape is shown for reference.

the free-surface where the presence of the corner field pulls the crack front backward. The angle at which the crack front intersects the free-surface is about 100°. Bazant and Estenssoro (1979) have reported that the corner field attains the $1/\sqrt{r}$ singularity when the crack front intersects the free-surface at 101° for $\nu = 0.3$. We also note that the overall shape of this crack front is similar to the steady state threading dislocation in an epitaxial film as shown by Freund (1990). For comparison, a crack front with a quarter-circular shape is also shown in Fig. 4.

The local K_I corresponding to the steady state crack front is shown in Fig. 5. The steady state K_I solution is nearly uniform along the crack front except near the interface ($x_3/t = 0$). Again, we note that the present fully cracked/penetrated model does not permit uniform K_I along the entire crack front since K_I must vanish at the interface regardless of the crack front shape. The variation of K_I from the straight crack front solution as well as the quarter-circular crack front solution are also shown for comparison. Interestingly, the quarter-circular configuration can be used as the first approximation for nearly constant K_I crack shape. The average value of K_I is $K_I^{ave}/\sigma_0\sqrt{t} \approx 1.03$ for the steady state crack front. This value is in good agreement with $K_I^{ave}/\sigma_0\sqrt{t} \approx 1.04$ obtained from an approximation formula given by Beuth (1991). Indeed all three cases shown in the figure have approximately the same K_I^{ave}. This is consistent with the fact that the total energy release rate of any crack front is equivalent to the total work required to open up a unit slice of crack far behind the leading edge.

In Fig. 6a, the crack opening of the steady state crack (as viewed from the top) is plotted at different slices through the thickness. For convenience, the displacements are magnified by $E/2\sigma_0$. On the film–substrate interface ($x_3/t = 0$), the opening is zero since there is no decohesion. Closer to the free-surface, the crack opening increases gradually as $x_3/t \to 1$. Unlike a through-crack in a plate, the maximum crack opening occurs just behind the crack front ($x_1/t \approx -1$) and the opening narrows further away from the tip. This behavior can be explained by bulging of the film behind the crack front as shown in Fig. 6b where the cross-section of crack on the $x_2/t = 0$ (crack center) plane is plotted. The bulging arises because the crack front is shifted toward the negative x_1 direction which leads to greater crack opening just behind the crack front. Ahead of the crack, film shrinkage

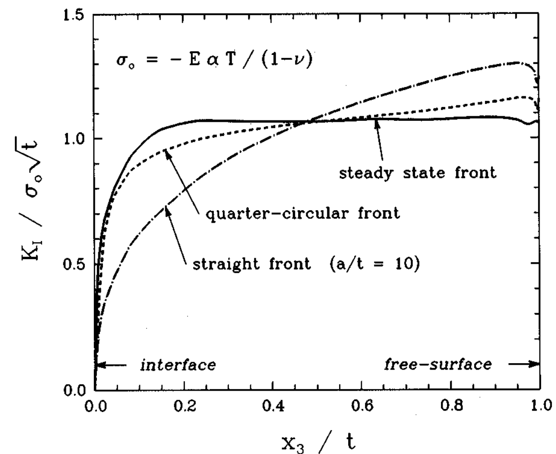

Fig. 5. Stress intensity factor for steady state crack front. The results of quarter-circular and straight crack front are also included for comparison. Note that $K_I^{ave}/\sigma_0\sqrt{t} = 1.03$ for the steady state crack front.

(Δt) rapidly approaches the solution under biaxial tension without the crack, $\Delta t = (1+\nu)\sigma_0 t/E$.

It is well known that for marginal or weakly adhered interfaces, the introduction of a cut in the film can lead to debonding. This problem was analyzed recently by Jensen et al. (1990) and Choi and Kim (1992) as the so-called "cut test" for adhesion. The debond driving force is largely dependent on the stress state at the interface. The contours of stresses from the steady state model (without any debonding) are shown in Fig. 7. The normal component σ_{33} tends to lift the thin film off the substrate while the shear components σ_{13} and σ_{23} tend to slide the thin film. It is interesting to observe that the shapes of high level stress contours for σ_{33} and σ_{23} are very similar to the shapes of decohered region shown by Jensen et al. (1990) and Choi and Kim (1992).

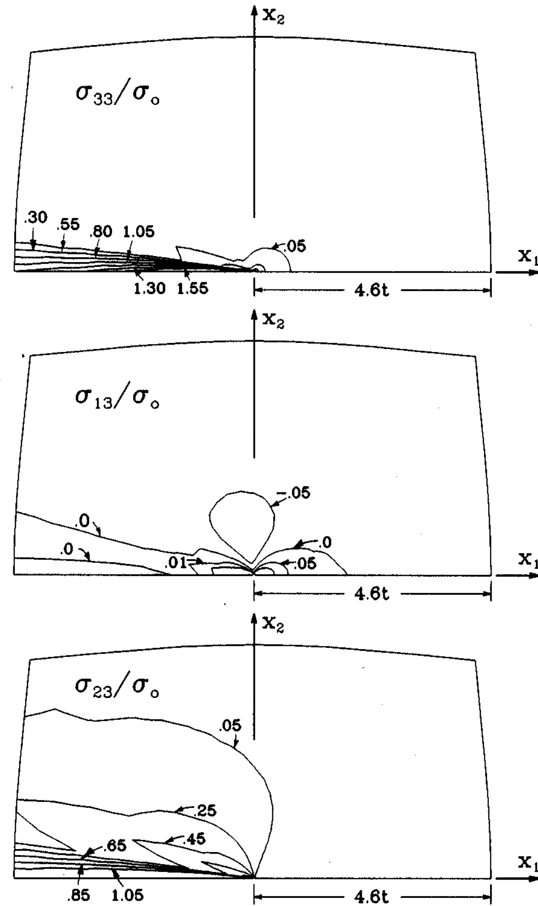

Fig. 7. Contours of stress components on the interface plane for bonded crack at steady state.

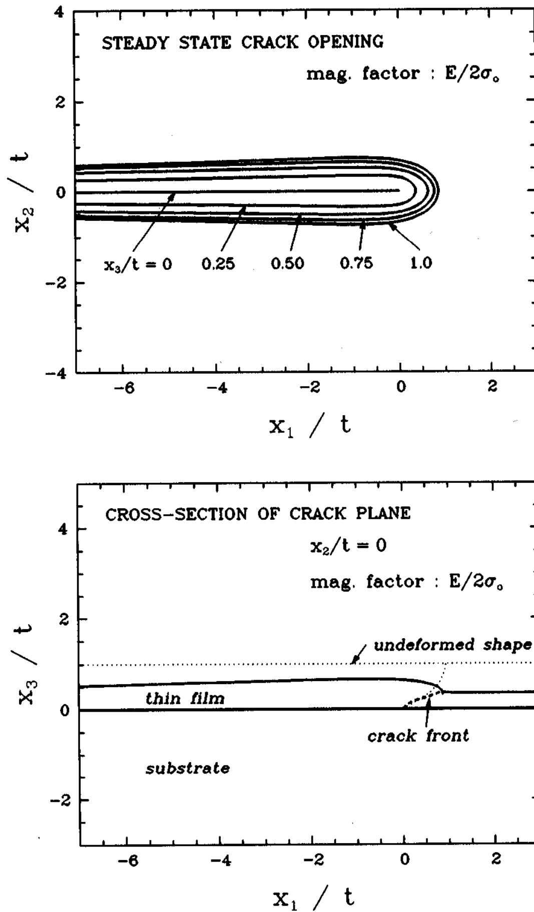

Fig. 6. (a) Top view of crack opening of steady state crack geometry. (b) Cross-sectional view of the crack. Deformation is magnified by $E/2\sigma_0$.

4. Analysis of debonded crack

4.1 Model

The previous section examined the case of a cut in the film where the crack boundary at the film–substrate interface was rigidly constrained

so that no debonding could occur. We now consider the effect of decohesion in the same cut with a simple decohesion model. In this model, the tip of the decohered region is always attached to the bottom of the leading crack front (no stand-off) as shown in Fig. 1b. Furthermore, debonding of the thin film from the substrate is assumed to occur in the region bounded by a constant angular ray, ω, above and below the crack behind the tip. Jensen et al. (1990) have shown that the criterion of stand-off is primary governed by the influence of Mode III contribution and the biaxial stress level. Their analysis showed that the debond opening angle, ω, can range $0° < \omega < \approx 45°$.

Since our primary interest is to determine the relationship between the amount of decohesion and the overall crack driving force (K_I), we did not remesh the model to determine a curved crack front corresponding to the steady state condition as done in Section 3.3. Thus, the crack front always remains straight and normal to the interface in the decohered model. The in-plane dimensions of thin film are large enough so that the solutions depend only on the thickness. The decohered condition is generated by removing the displacement boundary condition of the interface nodes between $\pm\omega$. Computations are carried out for $\omega = 15°$, 30° and 45°. Although the mixed-mode stress intensity factors along the edge of the decohered region are critical to the decohesion process, the present finite element mesh is not refined enough to compute these values accurately. Hence, we only consider the contribution to the strain energy release rate from K_I along the vertical front alone.

4.2. Effect of debond opening angle

The stress intensity factor along the leading crack front (not along the interfacial crack front between thin film and substrate) is computed for various debond opening angles, ω. The results shown in Fig. 8 indicate that the stress intensity factor along the crack front increases with angle of debonding. For a sufficiently long crack (e.g., $a/t = 10$), K_I along the crack front is independent of the crack length.

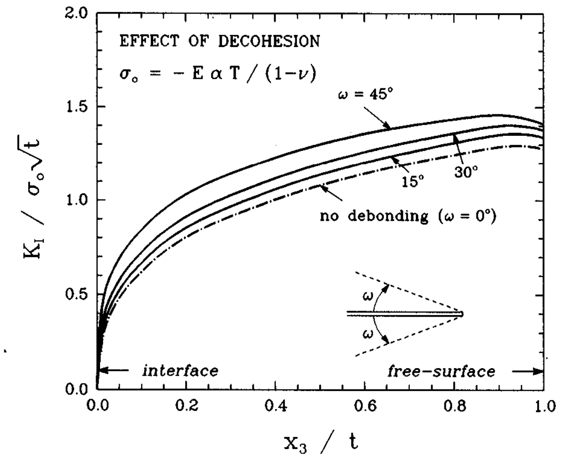

Fig. 8. Stress intensity factor for various angles of decohesion. Top view of the near crack tip region is depicted.

The mechanical process of thin film failure involving crack propagation and decohesion can be characterized as follows. Following Jensen et al. (1990), assume there is a steady state angle ω^{ss} under a given loading level, σ_0. Suppose a small increase or perturbation in ω occurs. Then K_I along the crack front increases according to the results shown in Fig. 8 and an extension in crack surface length a may follow. However, as the crack extends, the decohesion trails the crack tip and ω becomes smaller. Eventually, K_I decreases as ω is lowered to ω^{ss} and the crack arrests. Further extension can take place only if additional debonding occurs, leading to an increase in ω, and, therefore an increase in K_I. Although the actual process is likely to be influenced by other factors, this illustrates a simple interplay between the crack propagation and decohesion. Furthermore, it supports the existence of a stable equilibrium state for ω^{ss} for a crack with sufficiently large a. Closer experimental and analytical studies are warranted for more precise understanding of this process.

Crack opening of the decohered model is shown in Fig. 9a. Unlike the preceding case of no decohesion in Section 3, the crack opening increases with distance behind the crack tip. The lifting of film along the crack plane is shown in Fig. 9b. Nearly monotonic increase in the lift is

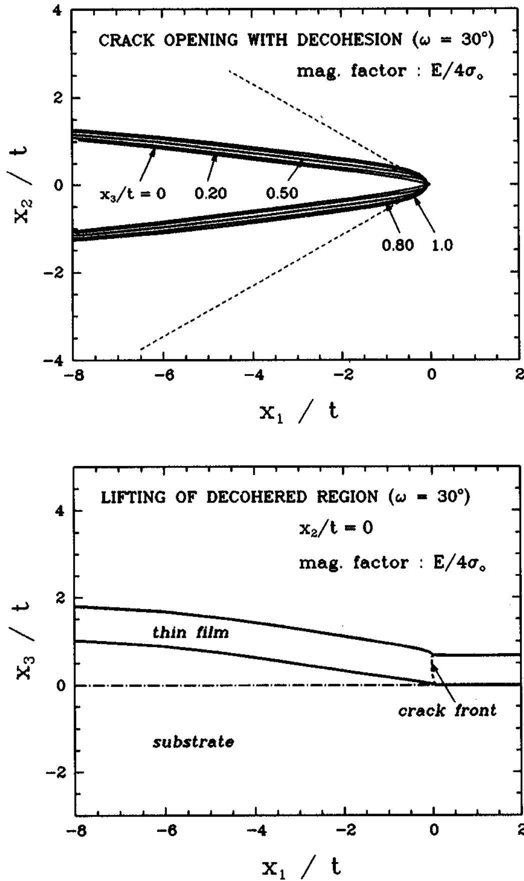

Fig. 9. (a) Top view of crack opening of decohered model with $\omega = 30°$. (b) Cross-sectional view on the crack plane. Deformation is magnified by $E/4\sigma_0$.

observed behind the crack front. In each figure, the deformation is magnified by $E/4\sigma_0$.

As stated earlier, the mixed-mode stress intensity factors along the decohered edges are not computed here. However, we have compared the 3-D stress field with the stress field obtained from a plane stress model of the decohered region. We have found that at distances greater than a few thicknesses away from the leading edge, the full geometrical field is close to the plane stress field and that its variation through the thickness is very small. This confirms the validity of solutions based on plane stress models of Jensen et al. (1990) and Choi and Kim (1992).

5. Closure

Important features associated with the 3-D deformation field of thin film fracture have been elucidated for the channeling and decohesion modes of failure. The steady state condition for film cracking is attained once the crack length is approximately twice the film thickness. The leading edge assumes a nearly parabolic shape through the film thickness in order to satisfy the constant K_I requirement almost everywhere except at the two ends of the front. Close to the leading edge, the field is highly three-dimensional in nature, but rapidly changes to a two-dimensional one at distances of 2–3t from the edge of the surface breaking cut. Thus, an understanding of the 3-D field becomes critical when the dominant mode is crack propagation/channeling with limited decohesion. The driving force for film debonding increases with crack opening angle and is traced to a significant level of stress at the film–substrate interface.

Availability of the detailed 3-D stress state and the driving force variation for the nonsteady crack, i.e., near initiation, will enable failure assessments of short cracks or defects in thin film structures. Material properties characterizing the resistance to film failure are the fracture toughness of the film and the critical energy release rate of the interface $G_c(\psi, \phi)$, corresponding to the mixed-mode phase angles, ψ and ϕ, for given film–substrate combination (Jensen et al., 1990; Nakamura, 1991). Work is in progress to establish relevant material and interface properties so that failure modes can be evaluated.

A natural extension of this study concerns the behavior of thin film cracks or defects in the presence of features which disturb the uniform biaxial residual stress state in the film. The results of such an analysis will be reported in a subsequent paper.

References

Bazant, Z.P. and L.F. Estenssoro (1979), Surface singularity and crack propagation, *Int. J. Solids Struct. 15*, 405.

Benthem, J.P. (1977), State of stress at the vertex of a quarter-infinite crack in a half-space, *Int. J. Solids Struct. 13*, 479.

Beuth, J.L. (1991), Cracking of thin bonded films in residual tension, Division of Applied Sciences Report, Harvard University, Cambridge, Mass.

Choi, H.C. and K.S. Kim (1992), Analysis of the spontaneous interfacial decohesion of a thin surface film, *J. Mech. Phys. Solids 40*, 75.

Cook, T.S. and F. Erdogan (1972), Stresses in bonded materials with a crack perpendicular to the interface, *Int. J. Eng. Sci. 10*, 677.

Dundurs, J. (1969), Edge-bonded dissimilar orthogonal elastic wedges under normal and shear loading, *J. Appl. Mech. 36*, 650.

Evans, A.G., M.D. Drory and M.S. Hu (1988), The cracking and decohesion of thin films, *J. Mater. Res. 3*, 1043.

Freund, L.B. (1990), The driving force for glide of a threading dislocation in a strained epitaxial layer on a substrate, *J. Mech. Phys. Solids 38*, 657.

He, M.Y. and J.W. Hutchinson (1989), Crack deflection at an interface between dissimilar elastic materials, *Int. J. Solids Struct. 25*, 1053.

Hu, M.S., M.Y. He and A.G. Evans (1991), Solvent-induced damage in polymide thin films, *J. Mater. Res. 6*, 1374.

Hutchinson, J.W. and Z. Suo (1991), Mixed mode cracking in layered materials, in: J.W. Hutchinson and T.Y. Wu, eds., *Advances in Applied Mechanics 28*, Academic Press, Orlando.

Jensen, H.W., J.W. Hutchinson and K.S. Kim (1990), Decohesion of a cut prestressed film on a substrate, *Int. J. Solids Struct. 26*, 1099.

Li, F.Z., C.F. Shih and A. Needleman (1985), A comparison of methods for calculating energy release rates, *Eng. Fract. Mech. 21*, 405.

Nakamura, T. (1991), Three-dimensional stress fields of elastic interface cracks, *J. Appl. Mech. 58*, 939.

Nakamura, T. and D.M. Parks (1988), Three-dimensional stress field near the crack front of a thin elastic plate, *J. Appl. Mech. 55*, 805.

Rice, J.R., Z. Suo and J.S. Wang (1990), Mechanics and thermodynamics of brittle interfacial failure in bimaterial systems, in: M. Ruhle, A.G. Evans, M.F. Ashby and J.P. Hirth, eds., *Metal-Ceramic Interfaces, Acta-Scripta Metallurgica Proceedings Series 4*, Pergamon Press, New York, p. 269.

Shih, C.F., B. Moran and T. Nakamura (1986), Energy release rate along a three-dimensional crack front in a thermally stressed body, *Int. J. Fract. 30*, 79.

Zak, A.R. and M.L. Williams (1963), Crack point singularities at a bi-material interface, *J. Appl. Mech. 30*, 142.